Available online at www.sciencedirect.com
ScienceDirect
Journal of Power Sources 162 (2006) 1346–1350
JOURNAL OF POWER SOURCES
www.elsevier.com/locate/jpowsour

Short communication

High capacity $Li[Li_{0.2}Ni_{0.2}Mn_{0.6}]O_2$ cathode materials via a carbonate co-precipitation method

D.-K. Lee [a], S.-H. Park [a,b], K. Amine [b], H.J. Bang [c], J. Parakash [c], Y.-K. Sun [a,*]

[a] *Department of Chemical Engineering, Center for Information and Communication Materials, Hanyang University, Seoul 133-791, Republic of Korea*
[b] *Electrochemical Technology Program, Chemical Engineering Division, Argonne National Laboratory, 9700 S. Cass Avenue, Argonne, IL 60439, USA*
[c] *Center for Electrochemical Science and Engineering, Department of Chemical and Environmental Engineering, Illinois Institute of Technology, 10 W. 33rd Street, Chicago, IL, USA*

Received 2 July 2006; received in revised form 31 July 2006; accepted 31 July 2006
Available online 12 September 2006

Abstract

Spherical $Li[Li_{0.2}Ni_{0.2}Mn_{0.6}]O_2$ has been synthesized by a carbonate co-precipitation method. The $Li[Li_{0.2}Ni_{0.2}Mn_{0.6}]O_2$ with a phase-pure and well-ordered layered structure was synthesized by heat-treatment of a spherical $(Ni_{0.25}Mn_{0.75})_3O_4$ precursor with $LiOH{\cdot}H_2O$. The average particle size of the $Li[Li_{0.2}Ni_{0.2}Mn_{0.6}]O_2$ powders was approximately 20 μm and the size distribution was quite narrow due to the homogeneity of the $(Ni_{0.25}Mn_{0.75})CO_3$. The $Li[Li_{0.2}Ni_{0.2}Mn_{0.6}]O_2$ electrode calcined at 900 °C delivered an initial discharge capacity of approximately 270 mAh g^{-1} in the voltage range of 2.0–4.6 V. The differential scanning calorimetry (DSC) results for the $Li[Li_{0.2}Ni_{0.2}Mn_{0.6}]O_2$ prepared at 900 °C showed a major exothermic reaction at 270 °C.

Keywords: Cathode material; Carbonate co-precipitation; ASI; Thermal stability; Lithium secondary batteries

1. Introduction

Because of their high energy density and power capability, lithium secondary batteries have become an important power source for portable electronic devices such as cellular phones, laptop computers and, more recently, hybrid electric vehicles (HEV) [1,2]. Presently, commercialized lithium-ion batteries use a $LiCoO_2$ cathode and a graphite anode. $LiCoO_2$ cathode materials are easy to prepare and have good electrochemical properties, however, due to the high cost and environmental problems resulting from cobalt, an intensive search for new electrode materials is being actively conducted. Recently, solid solutions between Li_2MnO_3 and $LiMn_{1-x}Ni_xO_2$ have become attractive because of the high capacity of over 200 mAh g^{-1} and enhanced safety at high voltages over 4.5 V [3–6]. Several methods have been used to prepare $Li[Ni_xLi_{(1/3-2x/3)}Mn_{(2/3-x/3)}]O_2$ and their derivative systems, such as hydroxide co-precipitation [7,8], sol–gel [9,10] and combustion [11]. However, with each of these methods it is hard to control the morphology, which lead to particle agglomeration. Therefore, selection of an appropriate preparation method is critical for attaining a highly pure final product.

In this study, a carbonate co-precipitation method was attempted to prepare spherical $Li[Li_{0.2}Ni_{0.2}Mn_{0.6}]O_2$ cathode materials by using a specialized continuous stirred tank reactor (CSTR). This method can control the spherical particle with a narrow particle size distribution and a highly homogeneous mixed transition metal. We report on the structural and electrochemical properties of a spherical $Li[Li_{0.2}Ni_{0.2}Mn_{0.6}]O_2$ using a $[Ni_{0.25}Mn_{0.75}]CO_3$ precursor prepared by a carbonate process.

2. Experimental

The $Li[Li_{0.2}Ni_{0.2}Mn_{0.6}]O_2$ material was synthesized by reacting stoichiometric amounts of a co-precipitated carbonate of manganese and nickel (cationic ratio of Ni:Mn = 1:3) with lithium hydroxide. The spherical $(Ni_{0.25}Mn_{0.75})CO_3$ was prepared as follows: an aqueous solution of $NiSO_4$ and $MnSO_4$ (cationic ratio of Ni:Mn = 1:3) with a concentration of 2.0 mol dm^{-3} was pumped into a continuous stirred tank reactor

* Corresponding author. Tel.: +82 2 2220 0524; fax: +82 2 2282 7329.
E-mail address: yksun@hanyang.ac.kr (Y.-K. Sun).

0378-7753/$ – see front matter © 2006 Elsevier B.V. All rights reserved.
doi:10.1016/j.jpowsour.2006.07.064

(CSTR, capacity 4 L) under CO_2 atmosphere. At the same time, Na_2CO_3 solution (aq.) of 2.0 mol dm^{-3} and desired amount of NH_4OH solution (aq.) as a chelating agent were also separately fed into the reactor. The concentration of the solution, pH (7.5), temperature (60 °C), and stirring speed of the mixture in the reactor was carefully controlled. At the initial stage of the co-precipitation reaction, the irregular secondary particles were formed and the irregular particles changed gradually into spherical particles by vigorous stirring for 12 h in the reactor. Then, the spherical $(Ni_{0.25}Mn_{0.75})CO_3$ particles were filtered and washed. The obtained spherical $(Ni_{0.25}Mn_{0.75})CO_3$ was dried at 110 °C and the carbonate was fired at 500 °C for 10 h to decompose the carbonate into an oxide compound. A mixture containing an excess amount of $LiOH{\cdot}H_2O$ and the de-carbonated powder, $(Ni_{0.25}Mn_{0.75})_3O_4$ (hereafter referred to as the precursor) was preheated at 500 °C for 10 h, and finally calcined at 700, 800, and 900 °C for 20 h in air.

Electrochemical charge–discharge tests were performed using a coin type cell (CR2032) with a current density of 20 mAh g^{-1} at 30 °C. The cell consisted of the positive electrode and the lithium metal as negative electrodes separated by porous polypropylene film. For the fabrication of the positive electrode, a mixture containing 20 mg of $Li[Li_{0.2}Ni_{0.2}Mn_{0.6}]O_2$ powder and 5 mg of conducting binder (3.3 mg of teflonized acetylene black (TAB) and 1.7 mg of graphite) was pressed on a 2.0 cm^2 stainless screen at 500 kg cm^{-2}. The electrolyte solution was 1 M $LiPF_6$ in a mixture of ethylene carbonate (EC) and diethyl carbonate (DEC) in a 1:1 volume ratio (CHEIL Industries Inc., Korea).

Powder X-ray diffraction (Rigaku, Rint-2000) employing Cu Kα radiation was used to identify the crystalline phase of the prepared powders. The prepared powders were also observed using scanning electron microscopy (SEM, JSM-6340F, JEOL). The chemical composition of the resulting powders was analyzed by atomic absorption spectroscopy AAS (Vario 6, Analytic-jena, Germany). The thermal stability of the prepared samples was investigated by differential scanning calorimetry (DSC, NETZSCH-TA4, Germany). The coin cells were charged to 4.6 V with a constant current density (0.1 C-rate) at 30 °C. The charged cells were then opened in an argon gas filled glove box and cathode electrodes were recovered from the cells. After opening the cell in the Ar-filled dry box, the electrode materials with wetted electrolyte were recovered from the current collector. DSC scanning was carried out at a scan rate of 5 °C min^{-1} from 50 to 350 °C.

3. Results and discussion

Fig. 1 shows that the powder X-ray diffraction (XRD) patterns of the precursor powder and $Li[Li_{0.2}Ni_{0.2}Mn_{0.6}]O_2$ materials calcined at various temperatures. The carbonate precursor consists of each transition metal carbonate of $NiCO_3$ (JCPDS No. 12-0771) and $MnCO_3$ (JCPDS No. 44-1472) having divalent valence. The $(Ni_{0.25}Mn_{0.75})CO_3$ precursor was able to be indexed to a hexagonal structure with a space group of *R*-3*c*. The diffraction peaks were quite broad due to the homogeneous mixed nano-scale particles. However, after firing at 500 °C,

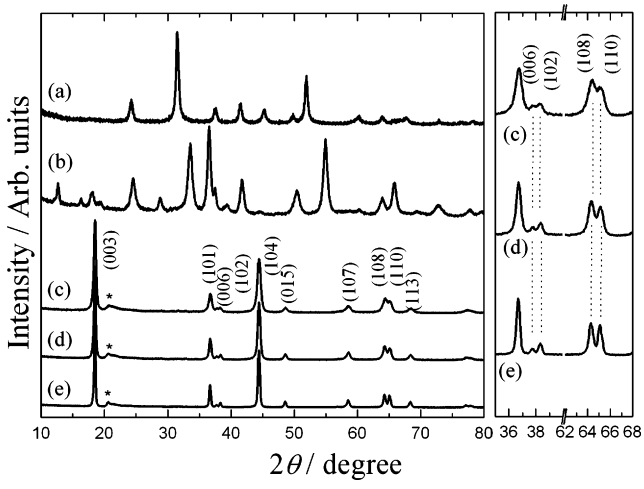

Fig. 1. X-ray diffraction patterns of (a) as-prepared $[Ni_{0.25}Mn_{0.75}]CO_3$, (b) pre-calcined at 500 °C, $[Ni_{0.25}Mn_{0.75}]_3O_4$, and $Li[Li_{0.2}Ni_{0.2}Mn_{0.6}]O_2$ powders were prepared at (c) 700 °C, (d) 800 °C, and (e) 900 °C.

the hexagonal carbonate powder transformed to $[NiMn]_3O_4$ (JCPDS No. 12-0269) with a cubic spinel structure, as can be seen from Fig. 1(b). From the AAS analysis, the chemical composition of the transition metals of Ni and Mn was 0.25 and 0.75. Calcination of the precursor with the lithium salt ($LiOH{\cdot}H_2O$) gave the phase-pure layered $Li[Li_{0.2}Ni_{0.2}Mn_{0.6}]O_2$ material as seen from Fig. 1(c)–(e). All the peaks can be indexed based on a hexagonal a-$NaFeO_2$ structure (space group: *R*3*m*, No. 166), except for a broad peak between 20° and 25°. These peaks might have been caused by Li_2MnO_3 composite with $Li[Ni_{0.5}Mn_{0.5}]O_2$ in the same layered structure. As the calcination temperature increased, separation of the (0 0 6)/(1 0 2) and (1 0 8)/(1 1 0) peaks became clearly distinct, which indicated the formation of a highly ordered lamellar structure [12]. Moreover, the intensity ratio of (0 0 3)/(1 0 4) peak increased slightly from 1.59 to 1.63 as the calcination temperature increases. Fig. 2 shows the scanning electron micrographs (SEM) images for the $(Ni_{0.25}Mn_{0.75})CO_3$ precursor and $Li[Li_{0.2}Ni_{0.2}Mn_{0.6}]O_2$ powders. It can be seen that the as-prepared carbonate particles have a spherical morphology with an average diameter of approximately 20 μm. Even though low magnification images are not shown in this paper, the final $Li[Li_{0.2}Ni_{0.2}Mn_{0.6}]O_2$ particles retain the spherical shape and the average particle size is nearly the same as the carbonate precursor even after being re-crystallized with lithium sources during high temperature calcination process. However, as calcination temperature increases, particles grew and surface morphology was changed from smooth surface to morphine like shape, due to the high temperature calcination. The particle size and surface morphological properties can give a high impact on their electrochemical and physical properties such as electrolyte wetting, surface resistance, rate properties, and tap density. Spherical shape of cathode materials has many advantages such as high packing density getting more energy, smaller specific surface area which is reduce reaction between cathode particle and electrolyte.

The variation of lattice constants, a_h and c_h, c/a ratio and volume of the $Li[Li_{0.2}Ni_{0.2}Mn_{0.6}]O_2$ material obtained at various

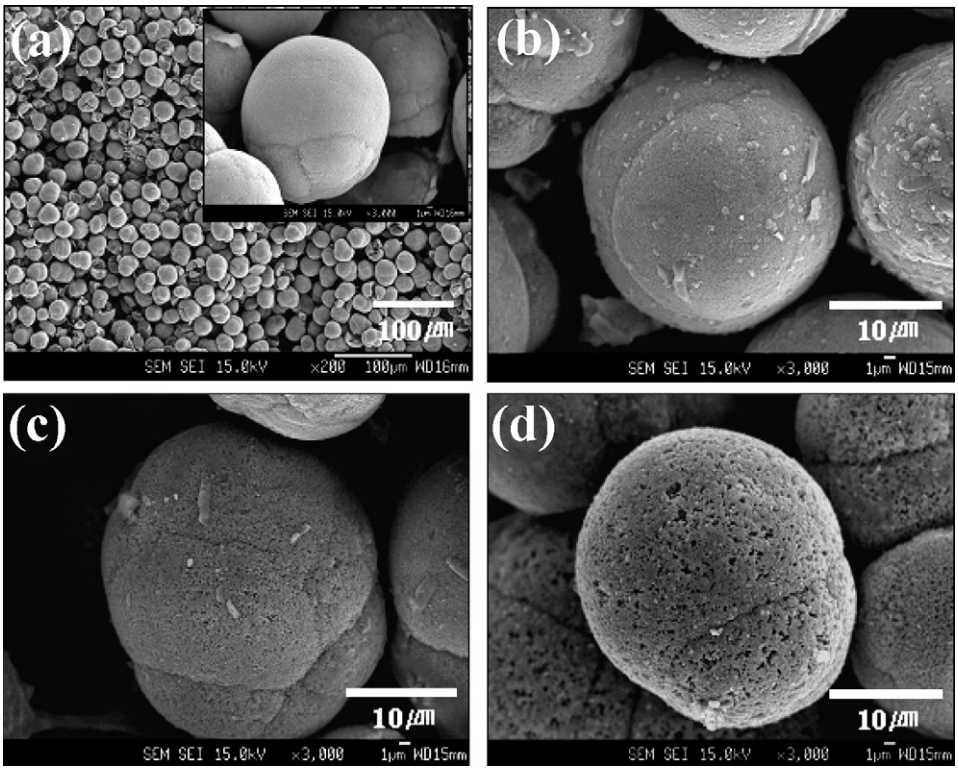

Fig. 2. Scanning electron microscopy (SEM) images: (a) $[Ni_{0.25}Mn_{0.75}]O_3$, inset figure is high magnification, and high magnification of $Li[Li_{0.2}Ni_{0.2}Mn_{0.6}]O_2$ powders were prepared at (b) 700 °C, (c) 800 °C, and (d) 900 °C.

calcination temperatures are shown in Table 1. As the calcination temperature increases, the lattice constants a_h and c_h, increased slightly from 2.863(3) to 2.867(2) Å, and 14.271(0) to 14.278(3) Å, respectively. The calculated lattice parameters were close to those of the reported values [13]. Moreover, *c*/*a* ratio of the all samples was greater than 4.9, a value is well known for material with layered characteristics. These lattice parameters and their increasing tendency with calcination temperature are in agreement with the results reported in literature for lithium–nickel–cobalt compounds [14,15]. The specific surface area for all the samples was measured by BET method and listed in Table 1. As increasing calcination temperature, the specific surface area decreased from 21.5 to 4.6 $m^2\,g^{-1}$ regardless of the same particle size.

Fig. 3(a) shows the first charge–discharge voltage profiles of the Li/$Li[Li_{0.2}Ni_{0.2}Mn_{0.6}]O_2$ cell by applying a constant current density of 20 mAh g^{-1} between 2.0 and 4.6 V. The irreversible capacity loss is only about 15–20 mAh g^{-1}, which is about 13–15% of the first charge capacity. With increasing calcination temperature, first columbic efficient were increased slightly from 85 to 87%. All cells had first irreversible capacity, of which voltage plateau was due to the extraction of lithium and oxygen starting at approximately 4.4 V, and their columbic efficiency is stabilized after second cycling. The irreversible capacity of all samples probably resulted from the oxygen loss from the structure during first cycling as well as the possible electrolyte decomposition since the onset potential of electrolyte is approximately 4.65 V, depending on electrolyte composition

Table 1
The variation of lattice constants, a_h and c_h, *c*/*a* ratio, volume and specific surface area (S_a) of the $Li[Li_{0.2}Ni_{0.2}Mn_{0.6}]O_2$ materials depending on the calcination temperature

	a_h (Å)	c_h (Å)	*c*/*a*	Volume (Å^3)	S_a ($m^2\,g^{-1}$)
700 °C	2.863(7)	14.271(0)	4.984(1)	101.32(5)	21.5(2)
800 °C	2.864(9)	14.276(3)	4.983(1)	101.47(6)	18.4(4)
900 °C	2.867(2)	14.278(3)	4.979(9)	101.65(4)	4.6(1)

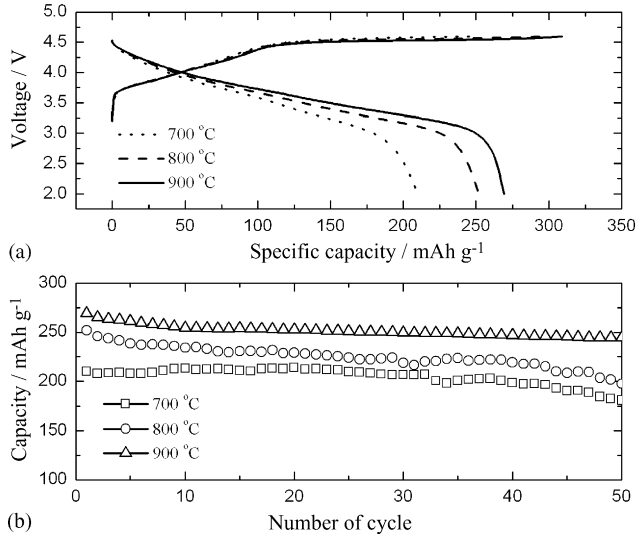

Fig. 3. (a) Charge/discharge curves and (b) variation in the specific discharge capacity as a function of number of cycles for the Li/$Li[Li_{0.2}Ni_{0.2}Mn_{0.6}]O_2$ cells with cut-off voltage 2.0 and 4.6 V.

[16]. Some portion of the irreversible capacity for all samples in Fig. 3 may come from the electrolyte oxidation. The most irreversible capacity may be related to the oxygen loss when the cell was charged above 4.45 V [16]. Fig. 3(b) shows the variations of the discharge capacities with cycling of the Li/Li[$Li_{0.2}Ni_{0.2}Mn_{0.6}$]O_2 calcined at various temperatures. The Li[$Li_{0.2}Ni_{0.2}Mn_{0.6}$]O_2 materials calcined at 700 and 800 °C delivered an initial discharge capacity of 210 and 250 mAh g^{-1}, respectively; the capacity retention of each cathode material after 50 cycles was only 79 and 85%, respectively. On the contrary, the Li[$Li_{0.2}Ni_{0.2}Mn_{0.6}$]O_2 calcined at 900 °C exhibited the initial capacity of 265 mAh g^{-1}, showing capacity retention of 92% after 50 cycles (discharge capacity: 244 mAh g^{-1}), which can be attributed to the enhanced structural stability reflected by clear separation of the (0 0 6)/(1 0 2) and (1 0 8)/(1 1 0) shown in Fig. 1. This may indicate that the cycling characteristics are affected by particles properties such as crystallite size, or particle morphology. As reported by Thackeray [17], high crystallinity is essential to obtain good electrochemical properties and to maintain its structural integrity during cycling.

Fig. 4 shows the differential capacity (dQ/dV) versus voltage (V) profiles of the Li/Li[$Li_{0.2}Ni_{0.2}Mn_{0.6}$]O_2 cells calcined at various temperatures. All samples have the large oxidation peak (starting at 4.45 V) in differential capacity during the first charge which is corresponds to the 4.5 V plateau in Fig. 3(a). Lu et al. explained the sharp 4.5 V peak (or 4.5 V plateau) resulted from the irreversible oxygen loss [16,18]. Recently, the mechanism of the first 4.5 V plateau has been well reported [18–20]: (i) lithium was extracted from Li layer, occurring a concurrent oxidation of transition metal of Ni below ~4.5 V and (ii) further lithium was extracted from transition metal layer above 4.5 V, which gave rise to concomitant oxygen release from Li_2MnO_3 component ($Li_2MnO_3 \rightarrow Li_2O + MnO_2$). After further cycling, the Li/Li[$Li_{0.2}Ni_{0.2}Mn_{0.6}$]O_2 cell showed two redox couple peaks at around 3.0 V (3.2 V in the case of 900 °C sample) and 3.8 V during charging process, which are attributed to the $Mn^{3+/4+}$ and $Ni^{2+/4+}$ redox couple, respectively [6]. Irregardless of synthesis temperature, the reduction peaks related to $Mn^{3+/4+}$ appeared at around 3.25 V region during first discharge process. As the cycling proceeds, this peak shifted to lower voltage region.

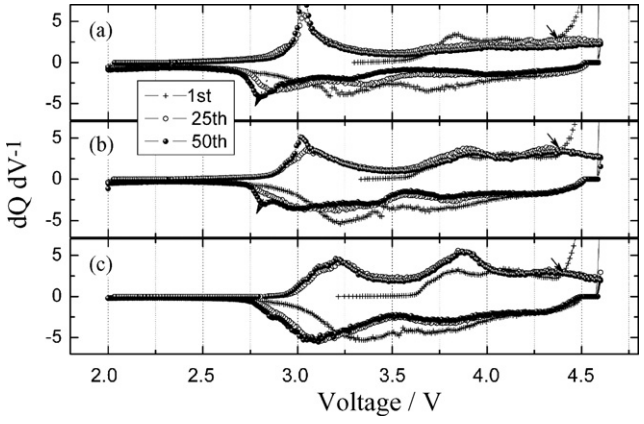

Fig. 4. Differential capacity vs. voltage of the Li/Li[$Li_{0.2}Ni_{0.2}Mn_{0.6}$]O_2 cells: (a) Calcined 700 °C, (b) 800 °C, and (c) 900 °C.

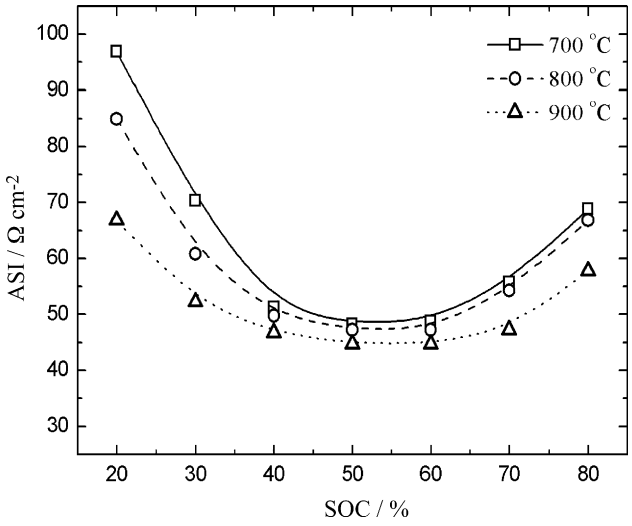

Fig. 5. Area specific impedance (ASI) vs. state of charge (SOC) for Li/Li[$Li_{0.2}Ni_{0.2}Mn_{0.6}$]O_2 cells: (a) 700 °C, (b) 800 °C, and (c) 900 °C samples.

The shift of peak position can be interpreted to subtle structural transition occurring in the cathode [16,18]. However, the Li[$Li_{0.2}Ni_{0.2}Mn_{0.6}$]O_2 electrode calcined at 900 °C showed limited shift of about 0.2 V and stable peak pattern comparing to other samples calcined at 700 and 800 °C. This behavior implies that for electrode calcined at 900 °C, noticeable structural degradation does not take place during the cycling process. It was also thought that the enhanced structural stability by the high temperature calcination leads to superior capacity retention as shown in Fig. 3(b).

Fig. 5 shows the area specific impedance (ASI) of the Li/Li[$Li_{0.2}Ni_{0.2}Mn_{0.6}$]O_2 cells as a function of state of charge (SOC, cut-off voltage is 2.0–4.6 V). The ASI were calculated by time dependent resistance applied during galvanostatic cycling which can be written by ($A\Delta V$)/I, where A is the cross-sectional area of electrode (2 cm^2), ΔV the voltage variation during current interruption for 60 s at each SOC, and I is the current (0.2 mA cm^{-2}). The ASI values slightly decrease as calcination temperature increases, which might be originated from well ordered layer structure.

In order to determine thermal stability of the prepared electrode, differential scanning calorimetry (DSC) was carried out as shown in Fig. 6. Usually, thermal decomposition properties were affected by state of delithiation, synthesis method, preparation conditions, average particle size, size distribution and the kinds of electrolyte. The Li_y[$Li_{0.2}Ni_{0.2}Mn_{0.6}$]O_2 samples were charged to 4.6 V versus Li metal in 1 M $LiPF_6$ in EC:DEC (1:1 by volume) electrolyte. The DSC experiments used screw type Pt tubes in order to avoid leaking of pressurized electrolyte. The onset temperature of exothermic peaks of the Li_y[$Li_{0.2}Ni_{0.2}Mn_{0.6}$]O_2 samples calcined at 700, 800, and 900 °C were 195, 205, and 278 °C and their amounts of heat generation were 428, 441 and 394 J g^{-1}, respectively. It is noticeable that the onset temperature of the 900 °C sample shifted from 195 to 278 °C compared with 700 °C sample. The drastic change of the onset temperature of the exothermic reaction on DSC results is not clear yet. One of plausible explanations is that

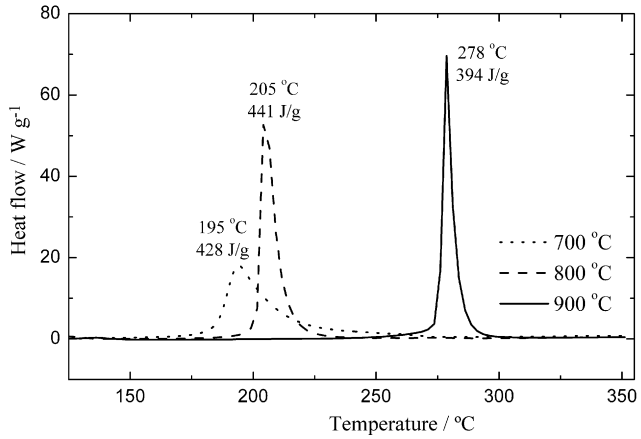

Fig. 6. Differential scanning calorimetry (DSC) profiles of Li/Li_y[$Li_{0.2}Ni_{0.2}Mn_{0.6}$]O_2 electrodes were charged at 0.1 C-rate to 4.6 V.

the stable crystal structure of the sample calcined at 900 °C generated less oxygen amount at higher temperature which reacts with EC and DEC in the electrolyte. Dahn et al. also reported the DSC results of the lithium excess cathode which show the multiple exothermic reaction peaks locating from 220–230 to 270–290 °C, depending on charge cut-off voltage [21]. It is possible that the samples prepared at relatively low temperatures (700 and 800 °C) still maintain $LiCoO_2$ like structure which give an exothermic reaction on DSC at around 200 °C resulting from EC combustion reaction with O_2 generated from the structure. The lattice parameters (*c*) of the samples (700 and 800 °C) shown in Table 1 was slightly larger than that of 900 °C sample. The larger values of *C*-axis of the samples (700 and 800 °C) imply that the repulsion between the oxygen layers is stronger than 900 °C sample, leading to the more and easier oxygen extraction from the host structure. The rapid oxidation peaks (as indicated by arrows) corresponding to the oxygen extraction on the first charge can be observed from differential capacity plot in Fig. 4. The onset of oxidation peaks of the 700 and 800 °C samples located at lower potential, compared to the 900 °C sample.

4. Conclusions

Spherical and mono-dispersed Li[$Li_{0.2}Ni_{0.2}Mn_{0.6}$]O_2 cathode materials with an average particle size of 20 μm were synthesized from co-precipitated spherical metal carbonate, [$Ni_{0.25}Mn_{0.75}$]CO_3. The samples prepared at 900 °C delivered a high discharge capacity of over 270 mAh g^{-1} between 2.0 and 4.6 V, showing good capacity retention of 92% after 50 cycles. The differential scanning calorimetry (DSC) result of the delithiated Li_x[$Li_{0.2}Ni_{0.2}Mn_{0.6}$]O_2 demonstrated superior thermal stability by showing a major exothermic peak at a much higher temperature compared to delithiated Li_xCoO_2 and Li_x[$Ni_{1-x}M_x$]O_2. The results of this work suggest that Li[$Li_{0.2}Ni_{0.2}Mn_{0.6}$]O_2 materials are a good candidate for the cathode material of high capacity lithium-ion batteries.

Acknowledgement

This work was supported by University IT Research Center Project.

References

[1] K. Amine, J. Liu, ITE Lett. 1 (2000) 59.
[2] K. Amine, C.H. Chen, J. Liu, M. Hammond, A. Jansen, D. Dees, I. Bloom, D. Vissers, G. Henriksen, J. Power Sources 97–98 (2001) 684.
[3] Z. Lu, D.D. MacNeil, J.R. Dahn, Electrochem. Solid State Lett. 4 (2001) A191.
[4] B. Ammundsen, J. Desilvestro, R. Steiner, P. Pickering, in: Proceedings of the 10th International Meeting on Lithium Batteries, vol. 97–98, Como, Italy, May 28–June 2, 2000.
[5] J.-H. Kim, C.S. Yoon, Y.-K. Sun, J. Electrochem. Soc. 150 (2003) A538.
[6] Z. Lu, J.R. Dahn, J. Electrochem. Soc. 149 (2002) A815.
[7] D.A.R. Barkhouse, J.R. Dahn, J. Electrochem. Soc. 152 (2005) A746.
[8] J. Jiang, K.W. Eberman, L.J. Krause, J.R. Dahn, J. Electrochem. Soc. 152 (2005) A1879.
[9] S.-H. Park, Y.-K. Sun, J. Power Sources 119–121 (2003) 161.
[10] S.-S. Shin, Y.-K. Sun, K. Amine, J. Power Sources 112 (2002) 634.
[11] Y.J. Park, M.G. Kim, Y.-S. Hong, X. Wu, K.S. Ryu, S.H. Chang, Solid State Commun. 127 (2003) 509.
[12] A. Rougier, P. Gravereau, C. Delmas, J. Electrochem. Soc. 143 (1996) 1168.
[13] R.D. Shannon, Acta Crystallogr., Sect. A: Cryst. Phys., Diffr., Theor. Gen. Crystallogr. 32 (1976) 751.
[14] T. Ohzuku, A. Ueda, M. Kouguchi, J. Electrochem. Soc. 142 (1995) 4033.
[15] B.J. Hwang, Y.W. Tsai, C.H. Chen, R. Santhanam, J. Mater. Chem. 13 (2003) 1962.
[16] Z. Lu, J.R. Dahn, J. Electrochem. Soc. 149 (2002) A815.
[17] M.M. Thackeray, J. Electrochem. Soc. 142 (1995) 2558.
[18] Z. Lu, L.Y. Beaulieu, R.A. Donaberger, C.L. Thomas, J.R. Dahn, J. Electrochem. Soc. 149 (2002) A778.
[19] S.-H. Kang, Y.-K. Sun, K. Amine, Electrochem. Solid State Lett. 6 (2003) A183.
[20] C.P. Grey, W.-S. Yoon, J. Reed, G. Ceder, Electrochem. Solid State Lett. 7 (2004) A290.
[21] Z. Lu, D.D. MacNeli, J. Dahn, Solid State Lett. 4 (2001) A191.